

How well known is the compressibility of nuclear matter?

J. Margueron¹ and E. Khan^{2,3}

¹*International Research Laboratory on Nuclear Physics and Astrophysics,
Michigan State University and CNRS, East Lansing, MI 48824, USA*

²*Université Paris-Saclay, CNRS/IN2P3, IJCLab, 91405 Orsay, France*

³*Institut Universitaire de France (IUF)*

(Dated: March 16, 2026)

The most accurate approach to determine the compressibility of nuclear matter remains the one based on microscopic Energy Density Functionals (EDFs). Recent analyses yield a value for nuclear incompressibility modulus $K_{\text{sat}} = 240 \pm 20$ MeV, defined in nuclear matter as the second derivative of the energy per particle at saturation density. However, we demonstrate that the compressibility modulus can be reduced to values shifted by four times the suggested uncertainty, i.e., $K_{\text{sat}} \approx 160$ MeV, by providing examples based on models where the second derivative (K_{sat}) and third derivative (Q_{sat}) of the energy per particle at saturation density can be independently varied, while the experimental binding energies, charge radii, and ISGMR data in ^{120}Sn and ^{208}Pb are enforced. The present work suggests a new methodology to access the compressibility of nuclear matter from nuclear experiments, still based on microscopic models, but using EDFs containing more flexibility than the ones employed up to now. Consequences of our results for nuclear matter at supra-saturation density are also discussed by exploring the quarkyonic cross-over. We predict that, for our models with low values for K_{sat} , the quark onset density has to be low for neutron stars to exist.

I. INTRODUCTION

The knowledge of the equation of state (EoS) for dense nuclear matter is instrumental for the understanding of astrophysical signals emitted from neutron stars (NSs) as well as gravitational waveforms originating from the fusion of two compact stars, see for instance Refs. [1, 2]. For symmetric matter (SM), an accurate probe of the density dependence of the energy per particle is the Isoscalar Giant Monopole Resonance (ISGMR) since it is known to be related to the incompressibility modulus of nuclear matter K_{sat} as analyzed in Ref. [3] for instance. Although not directly observable, the value of K_{sat} has been used as a constraint to elaborate specific Energy Density Functional (EDF) models. Originally suggested to be around 210 MeV in the 80's [3], it was then pointing towards larger values (260–270 MeV) for analyses based on the relativistic mean field approach [4], and the most recent suggested value from Ref. [5] is now $K_{\text{sat}} = 240 \pm 20$ MeV. However, the lack of precision in the final value of K_{sat} may pinpoint a caveat in the method.

Indeed, the relation between the ISGMR measurement in nuclei and the value of K_{sat} in uniform matter is not straightforward. It was investigated in several studies, see for instance the additional works in Refs. [6–16]. Moreover, it has been underlined that the density-dependence of the nuclear incompressibility impacts its determination at saturation density [17–20]. To picture this, it could be recalled that in ^{208}Pb , the majority of nucleons (about 2/3 of the total) are localized at its surface, i.e., at sub-saturation density as shown for instance in Ref. [18]. Therefore, nuclear experimental properties are influenced by the properties of nuclear matter below saturation density. Although this qualitative argument is to be taken with caution, it suggests that the

ISGMR strength in ^{208}Pb may not only probe the incompressibility at saturation density $\rho_{\text{sat}} \approx 0.155 \text{ fm}^{-3}$, see Refs. [21, 22], but also the density dependence $K(\rho)$ of the incompressibility from the saturation density to about 2/3 of its value, see Refs. [18, 19] for more details.

The present work is organized in the following way: the nuclear empirical parameters K_{sat} and Q_{sat} are introduced and discussed in Sec. II, then the theoretical predictions for the ISGMR are discussed in Sec. III, and the comparison between theoretical predictions and experimental measurements is shown in Sec. IV. Finally, we discuss the consequences of our analysis for the dense matter EoS and the possible onset of a phase transition at low density. Conclusions and outlooks are given in Sec. VI.

II. THE NUCLEAR EMPIRICAL PARAMETERS K_{sat} AND Q_{sat}

At lowest order, the density dependence of the compressibility modulus is driven by the skewness parameter Q_{sat} , defined as the third derivative of the energy per particle at saturation density, see Ref. [21] for more details, although more dedicated quantities could be considered, such as the derivative of the incompressibility at the density $\rho_c = 0.11 \text{ fm}^{-3}$, the so-called parameter $M_c = 3\rho_c K'(\rho)$ introduced in Ref. [19]. Therefore, ISGMR measurements shall be correlated with at least two properties characterizing nuclear matter and reflecting the densities in nuclei. The simultaneous role of both K_{sat} and Q_{sat} is illustrated by their correlation, as in Fig. 5 of Ref. [19] and reproduced in Fig. 1 (colored squares) of the present paper. Results from various Skyrme, Generalized Skyrme [26], Gogny, Fayans [23–25]

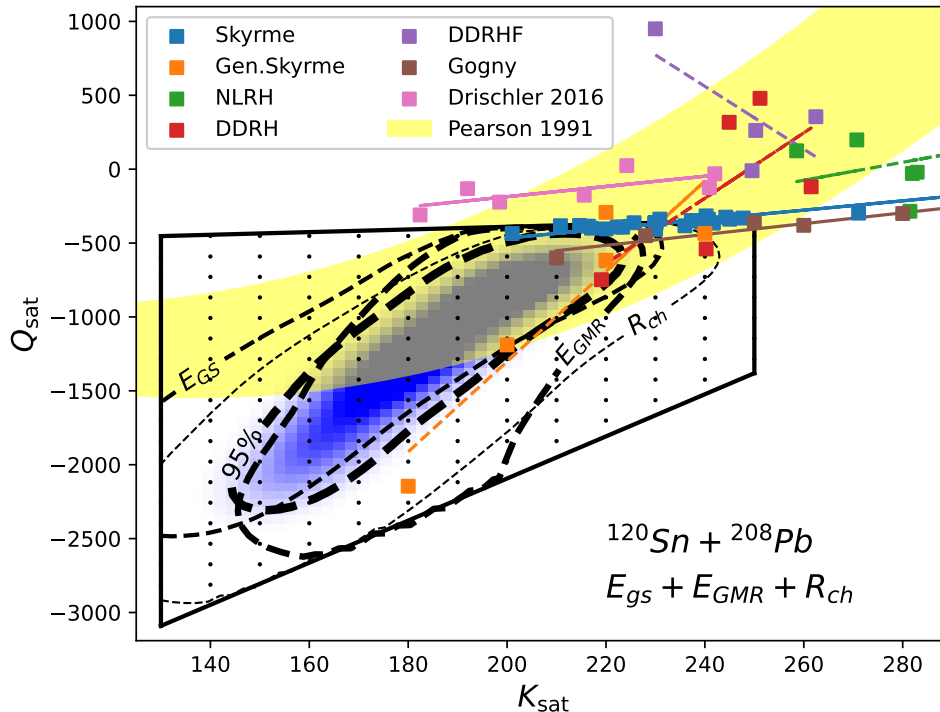


FIG. 1: Domain in $(K_{\text{sat}}, Q_{\text{sat}})$ parameter space for the EDFs (squares and lines): Skyrme, Generalized Skyrme, RMF (NLRHF and DDRH), DDRHF, Gogny, MBPT 2016 and Fayans EDFs [23–25] (see text for details). The parameter space explored in the present study is shown in blue surface, while the 95% C.I. associated with the ground-state energy (E_{gs}), the charge radius (R_{ch}) and the ISGMR (E_{GMR}) are shown in dashed lines. The correlation suggested by Pearson [6] is shown in yellow.

EDFs, Many-Body Perturbation Theory (Drischler 2016) based on χ EFT interactions calculated by Drischler [27] and relativistic EDFs are shown. The strong linear correlation found for each family of EDF, such as Skyrme, Fayans, and Gogny EDFs, shown with solid lines, means that setting K_{sat} defines Q_{sat} . This correlation is shown in Fig. 1 by the alignment of Skyrme EDFs (similarly for generalized Skyrme, Fayans, Gogny, and χ EFT EDFs). This strong correlation freezes the density dependence of the incompressibility, forbidding the free exploration of $(K_{\text{sat}}, Q_{\text{sat}})$ parameter space. For the other EDFs, i.e., Density-Dependent Relativistic Hartree (DDRH) first introduced in Ref. [28], Non-Linear Relativistic Hartree (NLRH) suggested by [29], and Density-Dependent Relativistic Hartree-Fock (DDRHF) by [30], the correlation is weaker (dashed lines), but the explored domain of $(K_{\text{sat}}, Q_{\text{sat}})$ parameter space remains quite narrow in the figure. Note that Q_{sat} is identical to the parameter S discussed in Refs. [6, 7, 17]. This parameter is sometimes called the anharmonicity parameter, since it measures the deviation from the harmonic behavior around saturation density given by K_{sat} .

A broader exploration of $(K_{\text{sat}}, Q_{\text{sat}})$ parameter space shall be considered to better investigate the link between available nuclear data and the density dependence of the EoS around saturation density. It is therefore impor-

tant to break the tight correlation between K_{sat} and Q_{sat} observed so far, see Fig. 1 for instance. For this purpose, Skyrme EDFs with extended density dependence have been considered in the present analysis. Skyrme EDFs indeed provide a simple EDF model that describes a large variety of nuclear properties at low energy, see for instance Ref. [31], allowing clear and efficient interpretation of nuclear data. However, the purpose of the present paper is not to suggest an extension of Skyrme EDFs but instead to investigate models breaking the correlation between K_{sat} and Q_{sat} . These models provide counterexamples of the usual ones, and it will be shown in this analysis that models with compressibility modulus lower than the common expectation are possible.

III. THEORETICAL PREDICTIONS FOR THE ISO-SCALAR GIANT MONOPOLE RESONANCE (ISGMR) STRENGTH DISTRIBUTION

The predictions for the ISGMR, using fully microscopic approaches based on Skyrme EDFs, are performed within Constrained-HFB (CHFb) and QRPA approaches. The CHFb method, suggested in Ref. [32], is known to provide an accurate prediction of ISGMR centroid as found in Refs. [19, 33] by using sum rules. It allows for fast

calculations, which is an advantage for systematic calculations, as in the present analysis. The ISGMR energy is calculated as

$$E_{\text{ISGMR}} = \sqrt{\frac{m_1}{m_{-1}}}. \quad (1)$$

where k -th energy-weighted sum rule is defined as

$$m_k = \sum_i (E_i)^k |\langle i | \hat{Q} | 0 \rangle|^2, \quad (2)$$

with E_i the RPA excitation energy and $\hat{Q} = \sum_{i=1}^A r_i^2$ the isoscalar monopole transition operator.

The m_1 moment is calculated from the double commutator, using the Thouless theorem [34], namely $m_1 = 2(\hbar^2/m)A\langle r^2 \rangle$, where A is the number of nucleons, m nucleon mass, and $\langle r^2 \rangle$ rms radius evaluated for ground-state density provided by the considered EDF. The CHF approach has been considered in Refs. [14, 17, 32, 33] to obtain the m_{-1} moment. It consists in adding to EDF hamiltonian \hat{H}_{EDF} a constraint associated with isoscalar monopole operator, namely $\hat{H}_{\text{constr}} = \hat{H}_{\text{EDF}} + \lambda \hat{Q}$. The m_{-1} moment is then obtained from the derivative of the expectation value of the monopole operator on CHF solution $|\lambda\rangle$,

$$m_{-1} = -\frac{1}{2} \left[\frac{\partial}{\partial \lambda} \langle \lambda | \hat{Q} | \lambda \rangle \right]_{\lambda=0}. \quad (3)$$

In addition to the CHF approach, the QRPA has the advantage of providing the strength function, see for instance the spherical Skyrme-QRPA model presented in Ref. [37], where the whole residual interaction is considered and the QRPA equations are expressed in matrix form involving the A and B matrices [38]:

$$\begin{pmatrix} A_{\alpha\beta,\gamma\delta} & B_{\alpha\beta,\gamma\delta} \\ -B_{\alpha\beta,\gamma\delta}^* & -A_{\alpha\beta,\gamma\delta}^* \end{pmatrix} \begin{pmatrix} X_{\gamma\delta}^\nu \\ Y_{\gamma\delta}^\nu \end{pmatrix} = E_\nu \begin{pmatrix} X_{\alpha\beta}^\nu \\ Y_{\alpha\beta}^\nu \end{pmatrix}. \quad (4)$$

We first assess the compatibility between CHF and QRPA for a few extended Skyrme EDFs. A comparison between the CHF and the QRPA for E_{ISGMR} is given in Tab. I for ^{120}Sn and ^{208}Pb and for a set of four extended Skyrme EDFs among those considered in the present work, as described below. It illustrates that these two approaches provide values that are comparable within a theoretical uncertainty of ≈ 0.1 - 0.2 MeV. We obtained similar results with other extended Skyrme EDFs given in App. A.

The description of the ISGMR in both Sn and Pb nuclei is known to be one of the most stringent tests for EDFs. For instance, Refs. [39, 40] have recently shown that considering configurations mixing beyond 1particle-1hole improves the theoretical description of this data. Therefore, this data shall be considered, among others, to design new EDFs with extended density dependence.

For our demonstration, a term of the following form, $\frac{1}{6}t'_3(1 + x'_3 P_\sigma)\rho^{\gamma'}\delta(\vec{r}_1 - \vec{r}_2)$, where t'_3 , x'_3 and γ' are new

parameters and P_σ is the spin exchange operator, has been added to standard Skyrme EDFs. This new term can be justified as representing better the in-medium many-body forces than standard Skyrme EDFs. It generates contributions to both the Hartree-Fock field and the residual interaction, which are analogous to the ones generated by the usual density-dependent interaction, see Ref. [41].

In the case of the pairing channel (which matters for ^{120}Sn), we consider a mixed contact pairing interaction of the following form: $300 \text{ MeV fm}^{-3}[1 - 0.5(\rho/\rho_{\text{sat}})^{0.2}]\delta(r)$. This mixed pairing form impacts mostly the binding energy in ^{120}Sn . The parameter 0.5 influences the mass-number dependence of the pairing gap: an intermediate value between the two extremes (0 and 1) is adopted in Refs. [42] and [43]. The power of density, 0.2, may affect the appearance of neutron skins and halos as shown by [42]. The values of the pairing interaction parameters are fixed to get a pairing gap of about 1.25 MeV in ^{120}Sn with SLy4 Skyrme interaction. Note that the pairing interaction could also be completed with isovector terms, see Refs. [44] and [45]. For the calculation of charge radii, we consider spin-orbit and Darwin-Foldy contributions, which provide magnetic dipole moment and relativistic corrections to nuclear rms charge radius as shown by [31] and [46].

In this framework, nuclear empirical parameters (NEP) K_{sat} and Q_{sat} in symmetric matter (SM) are expressed in the following way

$$K_{\text{sat}} = \left(-\frac{3}{5} \frac{\hbar^2}{2m} + 6C_0^\tau \rho_{\text{sat}} \right) \left(\frac{3\pi^2}{2} \right)^{2/3} \rho_{\text{sat}}^{2/3} + 9(2C_0' + C_0''\rho) \rho_{\text{sat}}^2, \quad (5)$$

$$Q_{\text{sat}} = \left(\frac{12}{5} \frac{\hbar^2}{2m} - 6C_0^\tau \rho_{\text{sat}} \right) \left(\frac{3\pi^2}{2} \right)^{2/3} \rho_{\text{sat}}^{2/3} + 27(3C_0'' + C_0'''\rho) \rho_{\text{sat}}^2, \quad (6)$$

with $C_0^\tau = [3t_1 + (5 + 4x_2)t_2]/16$ and

$$C_0' = \frac{1}{16} \left[\gamma t_3 \rho_{\text{sat}}^{\gamma-1} + \gamma' t_3' \rho_{\text{sat}}^{\gamma'-1} \right], \quad (7)$$

$$C_0'' = \frac{1}{16} \left[\gamma(\gamma-1)t_3 \rho_{\text{sat}}^{\gamma-2} + \gamma'(\gamma'-1)t_3' \rho_{\text{sat}}^{\gamma'-2} \right], \quad (8)$$

$$C_0''' = \frac{1}{16} \left[\gamma(\gamma-1)(\gamma-2)t_3 \rho_{\text{sat}}^{\gamma-3} + \gamma'(\gamma'-1)(\gamma'-2)t_3' \rho_{\text{sat}}^{\gamma'-3} \right], \quad (9)$$

where combinations of these parameters are fixed by the saturation density ρ_{sat} , the binding energy at saturation E_{sat} , and the effective mass m_{sat}^*/m . Two additional parameters in SM, namely t_3' and γ' – since x_3' impacts only asymmetric matter – allow us to widely explore the NEPs K_{sat} and Q_{sat} , and to break the linear correlation among them shown in Fig. 1. Actually, large uncertainties for Q_{sat} , about ± 1 GeV, has been suggested in Refs. [19, 21, 47] and we explore a large range of values for K_{sat} , well outside the usual 220-260 MeV domain.

K_{sat}	Q_{sat}	CHFB	QRPA	t_0	x_0	t_3	x_3	γ	t'_3	x'_3	γ'
MeV	MeV	MeV	MeV								
^{120}Sn with $E_{\text{ISGMR}}^{\text{exp}} = 15.5 \pm 0.2$ MeV from [35]											
180	-1491	15.63	15.40	-1287	0.258	14634	1.04	0.80	-34183	0.666	2.40
180	-1412	15.63	15.39	-1264	0.235	21977	0.986	0.95	-33679	0.747	1.90
210	-470	15.66	15.58	-2162	0.585	13739	1.028	0.25	-2998	0.196	1.00
210	-522	15.75	15.65	-1840	0.511	13281	1.040	0.35	-4926	0.537	1.05
^{208}Pb with $E_{\text{ISGMR}}^{\text{exp}} = 13.5 \pm 0.2$ MeV from [36]											
180	-1531	13.23	13.34	-1320	0.284	12270	1.071	0.70	-41580	0.596	2.80
180	-1895	13.44	13.58	-1206	0.210	16057	1.074	0.95	-63869	0.747	2.85
210	-418	13.18	13.25	-2587	0.589	17180	0.860	0.20	-3449	-0.131	0.60
210	-540	13.36	13.43	-1708	0.462	16439	1.000	0.45	-8964	0.713	0.90

TABLE I: Comparison of the centroid energies defined as $E_{\text{ISGMR}} = \sqrt{m_1/m_{-1}}$ obtained for CHFB and QRPA approaches for several extended Skyrme EDFs for which the parameters t_0 , x_0 , t_3 , x_3 , t'_3 , x'_3 , γ and γ' are explicitly given. The other Skyrme parameters are the same as for SLy5, i.e., $t_1 = 483.13$, $x_1 = -0.328$, $t_2 = -549.4$, and $x_2 = -1.0$.

However, to limit the choice of parameters, we impose the same isovector NEPs of the SLy5 Skyrme EDF, namely the symmetry energy E_{sym} , and its density dependence L_{sym} . In the future, a wider domain of NEPs can be explored by releasing this limitation.

IV. COMPARISON BETWEEN THEORETICAL PREDICTIONS AND EXPERIMENTAL MEASUREMENTS

We consider the following three sets of experimental constraints: ISGMR centroid energy $E_{\text{ISGMR}}^{\text{exp}}(^{120}\text{Sn}) = 15.5 \pm 0.2$ MeV from Ref. [35] and $E_{\text{ISGMR}}^{\text{exp}}(^{208}\text{Pb}) = 13.5 \pm 0.2$ MeV from Ref. [36]; binding energy $B^{\text{exp}}(^{120}\text{Sn}) = -1020 \pm 5$ MeV and $B^{\text{exp}}(^{208}\text{Pb}) = -1636 \pm 2$ MeV from Ref. [48]; and charge radii are $R_{\text{ch}}^{\text{exp}}(^{120}\text{Sn}) = 4.65 \pm 0.02$ fm and $R_{\text{ch}}^{\text{exp}}(^{208}\text{Pb}) = 5.50 \pm 0.01$ fm from Ref. [49]. Systematic uncertainties are considered to fix the error bars. A likelihood probability $p = \exp(-\chi^2/2)$ is associated with each model, where χ^2 reflects the above-mentioned experimental constraints, see for instance recent Ref. [50] for details on the Bayesian approach. For each of these three sets of constraints, the 95% confidence interval is shown in Fig. 1 with different dashed lines. The thick dashed line in Fig. 1 is obtained by combining all three constraints: it delimits 95% of the probability distribution (shown in blue where deeper blue means larger probability). In the future, it would be interesting to analyze the impact of the surface energy (defined in semi-infinite matter) on the barrier heights in deformed nuclei and fission processes.

The key feature in our demonstration is that the new models, describing ISGMR, charge radii, and binding

energies in both ^{120}Sn and ^{208}Pb , explore wide values for Q_{sat} and K_{sat} , as it can be seen in Fig. 1. The $(K_{\text{sat}}, Q_{\text{sat}})$ correlation has been broadened, as aimed, namely the blue area compared to the squares representing EDF predictions. Note also the large agreement between our blue region and the yellow correlation suggested in Ref. [6] and reported in Ref. [7]. The yellow correlation is based on an empirical analysis of both experimental and theoretical results, and it is extrapolated to low values for K_{sat} that the original authors have not explored. The blue region shows that it is possible to obtain counterexamples exploring regions for the parameters K_{sat} and Q_{sat} that are unexplored by other approaches.

Extensions of standard Skyrme EDF have been suggested in the literature, see for instance Refs. [26, 51–54] and references therein. It is interesting to note that a model with a low value for $K_{\text{sat}} \approx 180$ MeV has been obtained in Ref. [26] but for a very specific value of Q_{sat} that makes this EDF out of the 95 % probability distribution (blue) domain, see Fig. 1. Models with values for K_{sat} as low as 180 MeV have also been obtained in Ref. [53] by fitting only nuclear ground state properties (without the ISGMR). However, the authors have not calculated the value of Q_{sat} associated with their values for K_{sat} , so we have not added these extensions to our analysis. Table I presents a set of extended Skyrme parameterizations obtained in the present analysis, and the complete list of models is given in App. A.

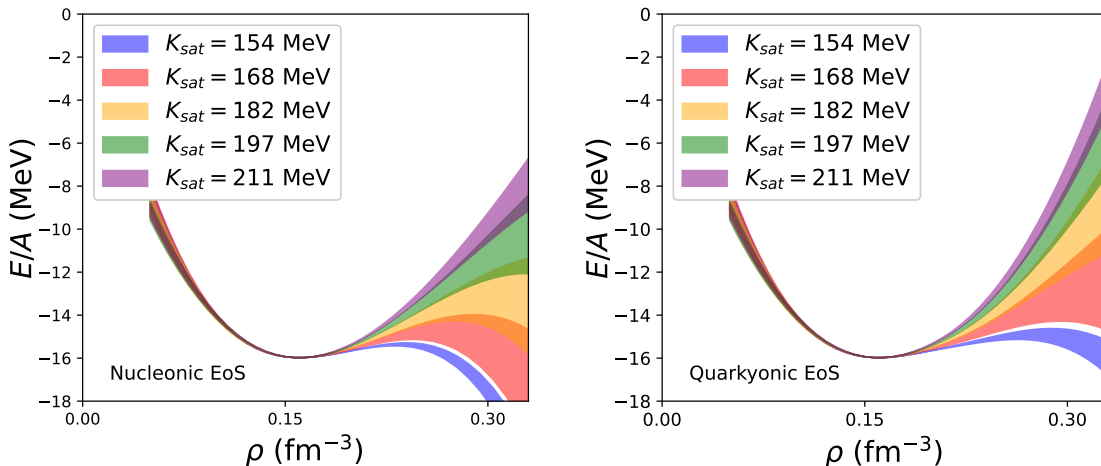


FIG. 2: Binding energy E/A for the nuclear equation of state based on the EDFs shown in Fig. 1. left: nucleonic models, right: quarkyonic models.

V. PREDICTION FOR THE EQUATION OF STATE ABOVE SATURATION DENSITY

Let us investigate the behavior of the EoS with low values for K_{sat} existing in the blue region of Fig. 1. These EoS are shown in Fig. 2 for SM as a function of the particle density. The range of Q_{sat} values associated with a value for K_{sat} in the validated domain (blue area on Fig. 1) is treated as uncertainties, giving rise to bands on the EoS. We also limit our density exploration to about $2\rho_{\text{sat}}$, since the properties of nuclei provide constraints only around ρ_{sat} and not very far above. It should be noted that nucleonic models with low K_{sat} values ($\lesssim 180$ MeV), explore also low Q_{sat} values, as shown in Fig. 1 (left). These models also predict that supra-saturation matter is more bound than matter at saturation density (nuclear matter collapse). However, a phase transition or a crossover, like the one provided by the quarkyonic model [55] and extended in asymmetric matter in Ref. [56], can modify this behavior above ρ_{sat} without impacting finite nuclei. Such an example of the quarkyonic model with a smooth transition to quark matter starting at 0.2 fm^{-3} is shown in the right panel of Fig. 2: a transition to quark matter starting above saturation density – therefore not modifying finite nuclei properties – could stabilize purely nucleonic models with low values of K_{sat} , except for $K_{\text{sat}} \lesssim 160$ MeV.

VI. CONCLUSIONS AND OUTLOOKS

In conclusion, it is shown that the uncertainty in K_{sat} obtained in recent data analyses, see for instance Ref. [10] and references therein, is underestimated. Examples are shown, see Fig. 1, which predict values for K_{sat} up to four sigma away from the standard one and still describe the ISGMR, binding energies, and charge radii data. While this result is based on well-known techniques, e.g., CHFB

and RPA as described above, the existence of these examples questions the common methodologies employing over-constrained models – with correlations among parameters – to analyze data in finite nuclei, like the ISGMR energy in ^{120}Sn and ^{208}Pb . These correlations are most probably artificial since these EDFs have been constructed by reducing as much as possible the number of parameters, as it is common in nuclear modeling. These induced correlations among parameters introduce a bias in the analysis of experimental data by limiting the free exploration of the parameter space. We suggest, instead, to analyze experimental data for ISGMR energies by employing flexible models where the parameters K_{sat} and Q_{sat} can be widely and independently varied. It is the condition for the uncertainties in K_{sat} and Q_{sat} to reflect those of the data, and not the internal correlations within the model.

In the case of the strong softening of nuclear matter above the saturation density suggested by some of our models and leading to nuclear matter collapse, a mechanism producing repulsion is necessary to stabilize neutron stars. We have explored one of them in our analysis: a low-density crossover between nuclear and quark matter provided by the quarkyonic model [55]. The present results show that precise measurements and accurate analyses of finite nuclear properties, such as, for instance, the ISGMR, can impact the onset of a new phase in the core of neutron stars.

ACKNOWLEDGEMENTS

We thank J.-P. Blaizot, W. Nazarewicz, and M. Urban for valuable discussions, and P.-G. Reinhard for providing us the values for K_{sat} and Q_{sat} predicted by Fayans EDFs and shown in Fig. 1. J.M. and E.K. are supported by the CNRS-IN2P3 MAC masterproject, and this work benefited from the support of the project RELANSE ANR-23-

CE31-0027-01 of the French National Research Agency (ANR). J.M. benefits from the LABEX Lyon Institute of Origins (ANR-10-LABX-0066).

Appendix A: Selected parameter sets

The complete list of extended Skyrme EDF parameter sets compatible with the experimental binding energies, charge radii, and ISGMR data in ^{120}Sn and ^{208}Pb is given in Table II.

-
- [1] K. Takami, L. Rezzolla, and L. Baiotti, Constraining the Equation of State of Neutron Stars from Binary Mergers, *Phys. Rev. Lett.* **113**, 091104 (2014), [arXiv:1403.5672 \[gr-qc\]](#).
- [2] M. Agathos, J. Meidam, W. Del Pozzo, T. G. F. Li, M. Tompitak, J. Veitch, S. Vitale, and C. Van Den Broeck, Constraining the neutron star equation of state with gravitational wave signals from coalescing binary neutron stars, *Phys. Rev. D* **92**, 023012 (2015).
- [3] J. Blaizot, Nuclear compressibilities, *Physics Reports* **64**, 171 (1980).
- [4] G. Lalazissis, S. Karatzikos, R. Fossion, D. P. Arteaga, A. Afanasjev, and P. Ring, The effective force nl3 revisited, *Physics Letters B* **671**, 36 (2009).
- [5] U. Garg and G. Colò, The compression-mode giant resonances and nuclear incompressibility, *Progress in Particle and Nuclear Physics* **101**, 55 (2018).
- [6] J. Pearson, The incompressibility of nuclear matter and the breathing mode, *Physics Letters B* **271**, 12 (1991).
- [7] S. Rudaz, P. J. Ellis, E. K. Heide, and M. Prakash, Anharmonicity of the nuclear matter ground state, *Physics Letters B* **285**, 183 (1992).
- [8] D. Vretenar, T. Nikšić, and P. Ring, A microscopic estimate of the nuclear matter compressibility and symmetry energy in relativistic mean-field models, *Phys. Rev. C* **68**, 024310 (2003).
- [9] B. K. Agrawal, S. Shlomo, and V. Kim Au, Nuclear matter incompressibility coefficient in relativistic and non-relativistic microscopic models, *Phys. Rev. C* **68**, 031304 (2003).
- [10] G. Colò, N. Van Giai, J. Meyer, K. Bennaceur, and P. Bonche, Microscopic determination of the nuclear incompressibility within the nonrelativistic framework, *Phys. Rev. C* **70**, 024307 (2004).
- [11] J. Piekarewicz, Why is the equation of state for tin so soft?, *Phys. Rev. C* **76**, 031301 (2007).
- [12] T. Li, U. Garg, Y. Liu, R. Marks, *et al.*, Isotopic dependence of the giant monopole resonance in the even- A $^{112-124}\text{Sn}$ isotopes and the asymmetry term in nuclear incompressibility, *Phys. Rev. Lett.* **99**, 162503 (2007).
- [13] J. Li, G. Colò, and J. Meng, Microscopic linear response calculations based on the Skyrme functional plus the pairing contribution, *Phys. Rev. C* **78**, 064304 (2008).
- [14] E. Khan, Role of superfluidity in nuclear incompressibilities, *Phys. Rev. C* **80**, 011307 (2009).
- [15] P. Veselý, J. Toivanen, B. G. Carlsson, J. Dobaczewski, N. Michel, and A. Pastore, Giant monopole resonances and nuclear incompressibilities studied for the zero-range and separable pairing interactions, *Phys. Rev. C* **86**, 024303 (2012).
- [16] W.-C. Chen and J. Piekarewicz, Building relativistic mean field models for finite nuclei and neutron stars, *Phys. Rev. C* **90**, 044305 (2014).
- [17] J. Blaizot, J. Berger, J. Dechargé, and M. Girod, Microscopic and macroscopic determinations of nuclear compressibility, *Nuclear Physics A* **591**, 435 (1995).
- [18] E. Khan, J. Margueron, and I. Vidaña, Constraining the nuclear equation of state at subsaturation densities, *Phys. Rev. Lett.* **109**, 092501 (2012).
- [19] E. Khan and J. Margueron, Determination of the density dependence of the nuclear incompressibility, *Phys. Rev. C* **88**, 034319 (2013).
- [20] J. Margueron and F. Gulminelli, Effect of high-order empirical parameters on the nuclear equation of state, *Phys. Rev. C* **99**, 025806 (2019).
- [21] J. Margueron, R. Hoffmann Casali, and F. Gulminelli, Equation of state for dense nucleonic matter from meta-modeling. I. Foundational aspects, *Phys. Rev. C* **97**, 025805 (2018).
- [22] C. Drischler, P. G. Giuliani, S. Bezoui, J. Piekarewicz, and F. Viens, A Bayesian mixture model approach to quantifying the empirical nuclear saturation point (2024), [arXiv:2405.02748](#).
- [23] P.-G. Reinhard and W. Nazarewicz, Toward a global description of nuclear charge radii: Exploring the fayans energy density functional, *Phys. Rev. C* **95**, 064328 (2017).
- [24] A. Miller, K. Minamisono, A. Klose, D. Garand, *et al.*, Proton superfluidity and charge radii in proton-rich calcium isotopes, *Nat. Phys.* **15**, 432 (2019).
- [25] S. Wang, A. Kanellakopoulos, X. Yang, S. Bai, *et al.*, Nuclear charge radii of germanium isotopes around $n = 40$, *Physics Letters B* **856**, 138867 (2024).
- [26] M. Farine, J. Pearson, and F. Tondeur, Nuclear-matter incompressibility from fits of generalized skyrme force to breathing-mode energies, *Nuclear Physics A* **615**, 135 (1997).
- [27] C. Drischler, K. Hebeler, and A. Schwenk, Asymmetric nuclear matter based on chiral two- and three-nucleon interactions, *Phys. Rev. C* **93**, 054314 (2016).
- [28] S. Typel and H. Wolter, Relativistic mean field calculations with density-dependent meson-nucleon coupling, *Nuclear Physics A* **656**, 331 (1999).
- [29] J. Boguta and A. Bodmer, Relativistic calculation of nuclear matter and the nuclear surface, *Nuclear Physics A* **292**, 413 (1977).
- [30] W.-H. Long, N. Van Giai, and J. Meng, Density-dependent relativistic hartree-fock approach, *Physics Letters B* **640**, 150 (2006).
- [31] M. Bender, P.-H. Heenen, and P.-G. Reinhard, Self-consistent mean-field models for nuclear structure, *Rev. Mod. Phys.* **75**, 121 (2003).
- [32] O. Bohigas, A. Lane, and J. Martorell, Sum rules for nuclear collective excitations, *Physics Reports* **51**, 267 (1979).
- [33] L. Capelli, G. Colò, and J. Li, Dielectric theorem within the Hartree-Fock-Bogoliubov framework, *Phys. Rev. C*

name	t_0	x_0	t_3	x_3	t'_3	x'_3	γ	γ'
SGMR160-3-75	-1343.43	0.2624	15081.47	0.9475	-32050.13	0.4905	0.75	2.25
SGMR160-3-80	-1306.21	0.2463	15382.97	0.9652	-38848.65	0.5260	0.80	2.40
SGMR160-3-85	-1273.67	0.2309	15764.64	0.9810	-47359.56	0.5584	0.85	2.55
SGMR170-2-75	-1413.99	0.2853	20480.78	0.8646	-22836.32	0.5570	0.75	1.50
SGMR170-2-85	-1335.11	0.2561	21367.45	0.9062	-28266.65	0.6229	0.85	1.70
SGMR170-2-90	-1302.71	0.2422	21970.49	0.9239	-31684.81	0.6514	0.90	1.80
SGMR170-3-80	-1296.59	0.2518	15008.60	1.0017	-36515.99	0.5915	0.80	2.40
SGMR170-3-85	-1265.15	0.2358	15401.25	1.0160	-44640.54	0.6229	0.85	2.55
SGMR170-3-90	-1237.40	0.2206	15867.61	1.0287	-54833.49	0.6514	0.90	2.70
SGMR180-2-95	-1263.71	0.2347	21976.53	0.9857	-33678.46	0.7469	0.95	1.90
SGMR180-3-65	-1407.54	0.3129	13884.45	0.9923	-19172.66	0.5551	0.65	1.95
SGMR180-4-50	-1543.63	0.3746	12169.66	0.9986	-14463.65	0.3938	0.50	2.00
SGMR180-4-60	-1412.33	0.3269	12028.10	1.0402	-24051.70	0.5084	0.60	2.40
SGMR180-4-70	-1320.07	0.2840	12270.04	1.0705	-41580.33	0.5964	0.70	2.80
SGMR190-2-75	-1381.15	0.3039	18925.97	0.9768	-19769.11	0.7210	0.75	1.50
SGMR190-2-85	-1309.55	0.2709	19913.86	1.0088	-24823.25	0.7786	0.85	1.70
SGMR190-3-45	-1672.91	0.4129	13752.03	0.9469	-8966.23	0.4213	0.45	1.35
SGMR190-3-55	-1506.49	0.3656	13351.30	1.0015	-12303.57	0.5523	0.55	1.65
SGMR190-4-65	-1351.56	0.3114	11821.12	1.0943	-28949.41	0.6480	0.65	2.60
SGMR190-4-70	-1310.65	0.2897	11998.58	1.1060	-38412.78	0.6868	0.70	2.80
SGMR200-2-45	-1753.62	0.4372	17685.93	0.8949	-10384.39	0.5474	0.45	0.90
SGMR200-2-60	-1509.82	0.3729	17320.35	0.9852	-13284.75	0.7185	0.60	1.20
SGMR200-2-80	-1328.60	0.2956	18622.84	1.0538	-20481.97	0.8503	0.80	1.60
SGMR200-2-90	-1268.50	0.2622	19839.29	1.0768	-26152.43	0.8949	0.90	1.80
SGMR200-4-50	-1506.68	0.3961	11431.68	1.0953	-11591.73	0.6152	0.50	2.00
SGMR210-2-50	-1618.86	0.4367	16281.96	1.0281	-9773.91	0.7729	0.50	1.00
SGMR210-2-65	-1432.05	0.3653	16626.77	1.0843	-13258.10	0.8932	0.65	1.30
SGMR210-2-75	-1348.31	0.3235	17371.16	1.1089	-16701.90	0.9453	0.75	1.50

TABLE II: Complete list of parameter sets. The other Skyrme parameters are the same as for SLy5, i.e., $t_1 = 483.13$, $x_1 = -0.328$, $t_2 = -549.4$, and $x_2 = -1.0$.

- 79, 054329 (2009).**
- [34] D. J. Thouless, Vibrational states of nuclei in the random phase approximation, *Nuclear Physics* **22**, 78 (1961).
- [35] T. Li, U. Garg, Y. Liu, R. Marks, *et al.*, Isoscalar giant resonances in the Sn nuclei and implications for the asymmetry term in the nuclear-matter incompressibility, *Phys. Rev. C* **81**, 034309 (2010).
- [36] M. Uchida, H. Sakaguchi, M. Itoh, M. Yosoi, *et al.*, Isoscalar giant dipole resonance in 208Pb via inelastic α scattering at 400 MeV and nuclear incompressibility, *Physics Letters B* **557**, 12 (2003).
- [37] G. Colò and X. Roca-Maza, User guide for the hfbcs-qrpa(v1) code (2021), [arXiv:2102.06562](https://arxiv.org/abs/2102.06562).
- [38] P. Ring and P. Schuck, *The nuclear many-body problem* (Springer-Verlag, New York, 1980).
- [39] E. Litvinova, Relativistic approach to the nuclear breathing mode, *Phys. Rev. C* **107**, L041302 (2023).
- [40] Z. Z. Li, Y. F. Niu, and G. Colò, Toward a unified description of isoscalar giant monopole resonances in a self-consistent quasiparticle-vibration coupling approach, *Phys. Rev. Lett.* **131**, 082501 (2023).
- [41] J. Dobaczewski, H. Flocard, and J. Treiner, Hartree-Fock-Bogolyubov description of nuclei near the neutron-drip line, *Nuclear Physics A* **422**, 103 (1984).
- [42] J. Dobaczewski, W. Nazarewicz, and P.-G. Reinhard, Pairing interaction and self-consistent densities in neutron-rich nuclei, *Nuclear Physics A* **693**, 361 (2001), radioactive Nuclear Beams.
- [43] J. Dobaczewski and W. Nazarewicz, Mean-Field and Pairing Properties of Exotic Nuclei: Exploring the Nuclear Landscape, *Progress of Theoretical Physics Supplement* **146**, 70 (2002), [arXiv:nuc1-th/0203038 \[nucl-th\]](https://arxiv.org/abs/nuc1-th/0203038).
- [44] J. Margueron, H. Sagawa, and K. Hagino, Effective pairing interactions with isospin density dependence, *Phys.*

- Rev. C* **77**, 054309 (2008).
- [45] M. Yamagami, J. Margueron, H. Sagawa, and K. Hagino, Isoscalar and isovector density dependence of the pairing functional determined from global fitting, *Phys. Rev. C* **86**, 034333 (2012).
- [46] B. V. Carlson, M. Dutra, O. Lourenço, and J. Margueron, Low-energy nuclear physics and global neutron star properties, *Phys. Rev. C* **107**, 035805 (2023).
- [47] G. Grams, R. Somasundaram, J. Margueron, and E. Khan, Nuclear incompressibility and speed of sound in uniform matter and finite nuclei, *Phys. Rev. C* **106**, 044305 (2022).
- [48] M. Wang, W. Huang, F. Kondev, G. Audi, and S. Naimi, The AME 2020 atomic mass evaluation (II). tables, graphs and references, *Chinese Physics C* **45**, 030003 (2021).
- [49] T. Li, Y. Luo, and N. Wang, Compilation of recent nuclear ground state charge radius measurements and tests for models, *Atomic Data and Nuclear Data Tables* **140**, 101440 (2021).
- [50] P. Giuliani, K. Godbey, E. Bonilla, F. Viens, and J. Piekarewicz, Bayes goes fast: Uncertainty quantification for a covariant energy density functional emulated by the reduced basis method, *Frontiers in Physics* **10**, 10.3389/fphy.2022.1054524 (2023).
- [51] T. Lesinski, K. Bennaceur, T. Duguet, and J. Meyer, Isovector splitting of nucleon effective masses, ab initio benchmarks and extended stability criteria for skyrme energy functionals, *Phys. Rev. C* **74**, 044315 (2006).
- [52] N. Chamel, S. Goriely, and J. M. Pearson, Further explorations of skyrme-hartree-fock-bogoliubov mass formulas. xi. stabilizing neutron stars against a ferromagnetic collapse, *Phys. Rev. C* **80**, 065804 (2009).
- [53] J. Erler, P. Klüpfel, and P.-G. Reinhard, Exploration of a modified density dependence in the skyrme functional, *Phys. Rev. C* **82**, 044307 (2010).
- [54] H. Gil, Y.-M. Kim, C. H. Hyun, P. Papakonstantinou, and Y. Oh, Analysis of nuclear structure in a converging power expansion scheme, *Phys. Rev. C* **100**, 014312 (2019).
- [55] L. McLerran and S. Reddy, Quarkyonic matter and neutron stars, *Phys. Rev. Lett.* **122**, 122701 (2019).
- [56] J. Margueron, H. Hansen, P. Proust, and G. Chanfray, Quarkyonic stars with isospin-flavor asymmetry, *Phys. Rev. C* **104**, 055803 (2021).